

The electrical conductivity of the solid electrolytes $\text{CaZr}_{1-x}\text{Sc}_x\text{O}_{3-\delta}$ ($x = 0.03$ and 0.08) was investigated as a function of temperature in a humid air atmosphere. The total electrical conductivity was separated into bulk and grain boundary conductivity. The bulk conductivity for $\text{CaZr}_{0.97}\text{Sc}_{0.03}\text{O}_{3-\delta}$ was found to be higher than that for $\text{CaZr}_{0.92}\text{Sc}_{0.08}\text{O}_{3-\delta}$. Using the oxygen partial pressure dependencies of electrical conductivity, the electron hole and ionic contributions to the total conductivity were distinguished. The oxides were found to be mixed ionic-electron hole conductors in air atmosphere and purely ionic conductors under reductive conditions. Transport numbers for ions and electron holes were calculated. At temperatures below 600°C , the oxides are expected to behave as nearly pure ionic conductors under air conditions. Although the ionic conductivities for the oxides are comparable, the ionic transport numbers for $\text{CaZr}_{0.97}\text{Sc}_{0.03}\text{O}_{3-\delta}$ were found to be higher than those for $\text{CaZr}_{0.92}\text{Sc}_{0.08}\text{O}_{3-\delta}$.

keywords: CaZrO_3 , solid electrolyte, electrical conductivity, transport number, bulk, grain boundary

© 2025, the Authors. This article is published in open access under the terms and conditions of the Creative Commons Attribution (CC BY) license (<http://creativecommons.org/licenses/by/4.0/>).

1. Introduction

Solid oxides have attracted extensive research interest across multiple disciplines due to their diverse physical and chemical properties, leading to broad applications in science and technology [1–5]. The discovery of high-temperature proton conductivity in solid oxides by H. Iwahara in the 1980s [6] has generated significant global scientific attention. This interest stems from the promising potential of these materials for electrochemical applications, particularly in solid oxide fuel cells (SOFCs) [7–10]. Proton-conducting oxides offer distinct advantages over conventional oxygen-ion conductors in SOFC applications, including lower operating temperatures and the prevention of fuel dilution by water vapor. Among the most extensively studied high-temperature proton conductors are perovskite-type materials, particularly doped BaCeO_3 , BaZrO_3 , and their solid solutions [11–13]. Although BaCeO_3 -based materials demonstrate high

proton conductivity, they suffer from chemical instability in CO_2 -containing atmospheres, leading to carbonate formation and material degradation. In comparison, BaZrO_3 -based materials demonstrate better chemical stability under similar conditions. However, they face two major challenges related to lower proton conductivity due to higher grain boundary resistance and difficulties in achieving full densification during sintering, which further compromises their electrochemical performance. CaZrO_3 -based oxides are other representatives of the electrolytes with the perovskite structure. Despite lower conductivities compared to barium-containing oxides, they show higher stability in CO_2 - and water-containing atmospheres. The most well-characterized material in this system is indium-doped CaZrO_3 , which has found practical application in hydrogen sensors for aluminum melts [14, 15]. Several studies have also examined the transport properties of yttrium-doped [16, 17] aluminum-doped [18, 19] and scandium-doped CaZrO_3 [20], demonstrating that these materials also exhibit proton conductivity and could serve as alternatives to In-doped CaZrO_3 . Among them, Sc-doped oxides were shown to

^a: Institute of High-Temperature Electrochemistry UB RAS, Ekaterinburg 620066, Russia

* Corresponding author: antonova_ek@list.ru

have the highest electrical conductivity values on a level comparable to that of In-doped oxides [21]. The authors of [22] have studied samples with Sc content up to 24 mol. %. It was shown that electrical conductivity decreases at the Sc content higher than 12 %. Similar results were obtained in [23], where the conductivity of $\text{CaZr}_{0.85}\text{Sc}_{0.15}\text{O}_{3-\delta}$ was found to be almost the same as for $\text{CaZr}_{0.9}\text{Sc}_{0.1}\text{O}_{3-\delta}$. In both studies, the samples with high Sc content were indicated as single phase, while the authors of [24] determined that the solubility limit of scandium in calcium zirconate was $x = 0.07\text{--}0.08$. It seems that the decrease in electrical conductivity for the compositions with high Sc content observed in [22, 23] can be related with the formation of additional low-conducting phases. Thus, it is of interest to investigate the electrical properties of CaZrO_3 doped with lower Sc content, as the literature provides detailed data only for 5 mol. % Sc-doped CaZrO_3 and limited information for 3 mol. % Sc-doped CaZrO_3 [25–27]. This study is devoted to the investigation of electrical conductivity of 3 and 8 mol. % Sc-doped CaZrO_3 ceramics with the focus on bulk and grain boundary conductivity, as well as on the contributions of ionic and electron hole conductivity.

2. Experimental

The samples $\text{CaZr}_{0.97}\text{Sc}_{0.03}\text{O}_{3-\delta}$ and $\text{CaZr}_{0.92}\text{Sc}_{0.08}\text{O}_{3-\delta}$ (hereinafter CZS3 and CZS8 respectively) were fabricated using conventional ceramic technology. ZrO_2 , CaCO_3 and Sc_2O_3 (all reagents of high-purity grade) were used for synthesis. Stoichiometric amounts of starting materials were mixed in a zirconia mortar with ethanol. After preliminary synthesis at 1200 °C, the pressed samples were finally sintered at 1800 °C for 1.5 hours in a vacuum furnace. After cooling, the samples were additionally annealed in air at 1200 °C for 24 hours. A more detailed description of the sample preparation methodology can be found in [25]. The phase purity of the obtained samples was studied by X-ray powder diffraction (D/MAX-2200, Rigaku). The microstructure peculiarities of the ceramics were investigated using scanning electron microscopy (MIRA 3LMU, Tescan). For electrical measurements, platinum electrodes were deposited on the surfaces of the electrolyte disk and sintered at 1000 °C for one hour. The electrical conductivity was determined via impedance spectroscopy (P-40X impedancemeter, Elins) in a temperature range of 200–800 °C in a humidified atmosphere ($p_{\text{H}_2\text{O}} = 3.17$ kPa). Humidification was achieved by bubbling the circulating gas through distilled water at room temperature. Measurements of the oxygen partial pressure dependencies of electrical conductivity were done in the temperature range of 650–800 °C in a

humidified atmosphere, spanning p_{O_2} values of 0.21 to 10^{-20} atm. Oxygen partial pressure was controlled using a Zirconia-M universal controller. Impedance spectra were collected with an AC amplitude of 20 mV over a frequency range of 1– 10^5 Hz. Further analysis of the impedance data was performed using the ZView software.

3. Results and discussion

3.1. Sample characterization

XRD results confirmed that obtained oxides were single-phase, crystallizing in the *Pcmn* space group (Figure 1(a)). The relative density of the obtained ceramics was of about 90 %. Figures 1(b)–(c) show SEM images of the obtained ceramics. The estimated average grain size was of about 3.3 and 1.1 μm for CZS3 and CZS8 respectively.

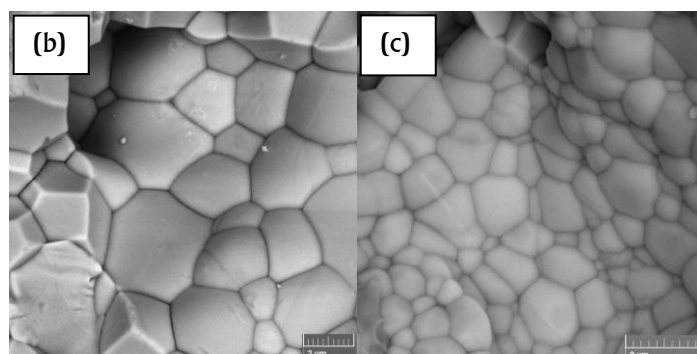
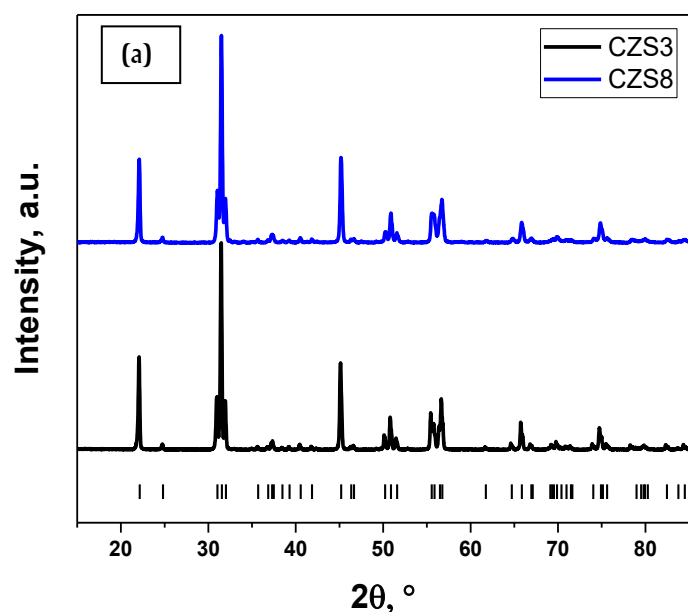


Figure 1 (a) XRD patterns for CZS oxides; (b) and (c) SEM images of the obtained ceramics, $\text{CaZr}_{0.97}\text{Sc}_{0.03}\text{O}_{3-\delta}$ and $\text{CaZr}_{0.92}\text{Sc}_{0.08}\text{O}_{3-\delta}$ respectively.

3.2. Electrical conductivity in air

Temperature dependencies of the electrical conductivity of the samples in wet air are depicted in

Figure 2. One can see that the electrical conductivity values for CZS3 and CZS8 are close, while the activation energy of the conductivity increases with increasing Sc content (Table I). Additionally, available literature data on electrical conductivity for CZS system are presented. It can be seen that the values are comparable. Slight differences can be attributed to different methods of conductivity measurements: literature data [25, 28] were obtained by the 4-probe DC method, while our data were measured by impedance spectroscopy.

At the temperatures below 700 °C, it became possible to distinguish bulk and grain boundary contributions to the total resistance. Figure 3 presents an example of an impedance spectrum for CZS3 at 500 °C. Two semicircles corresponding to bulk resistance and grain boundary resistance are clearly observable. Thus, the impedance data were analyzed using an equivalent circuit consisting of two serially connected parallel combinations of R (ohmic resistance) and CPE (constant phase element) elements, referred to as the RQ -circuit. An example of the spectra analysis, including partial contributions, is provided in Figure 3. Figure 4 displays the temperature dependencies for obtained bulk and grain boundary conductivities for CZS3 and CZS8.

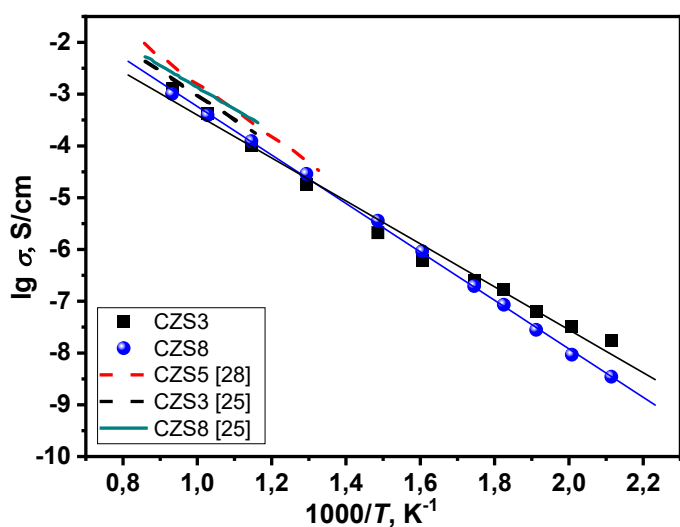


Figure 2 Temperature dependencies of electrical conductivity for CZS ceramics in wet air.

Table 1 – Activation energy values for total, bulk, and grain boundary conductivity.

Composition	E_a , kJ/mol		
	σ_{bulk}	σ_{gb}	σ_{tot}
CZS3	71 ± 1	84 ± 4	83 ± 3
CZS8	74 ± 2	100 ± 1	97 ± 1

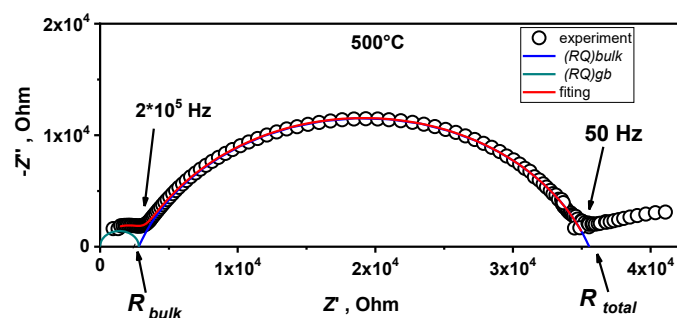


Figure 3 An example of an analysis of the impedance spectrum (CZS3 at 500 °C in wet air atmosphere).

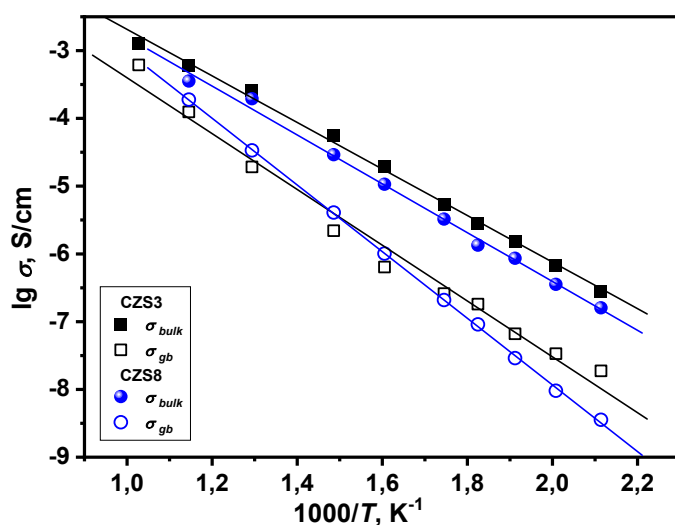


Figure 4 Temperature dependencies of bulk and grain boundary conductivity for CZS ceramics in wet air.

The corresponding values of activation energy are listed in Table I. It can be seen that bulk conductivity for CZS3 is slightly higher than that of CZS8 with close values of activation energy. The grain boundary conductivities are comparable; their dependencies have different slopes due to the difference in activation energies and intersect at the temperature of about 300 °C. For both oxides, the grain boundary conductivity is lower than the bulk conductivity, thus determining the total conductivity of the materials.

3.3. Electrical conductivity vs pO_2

In order to determine the nature of the electrical conductivity of CZS oxides, measurements of electrical conductivity as a function of oxygen partial pressure were performed. Figure 5 illustrates the resulting pO_2 dependencies. It is evident that for both oxides, electrical conductivity decreases with the reduction of oxygen partial pressure under oxidative conditions, while it is almost constant under reductive conditions. Such a

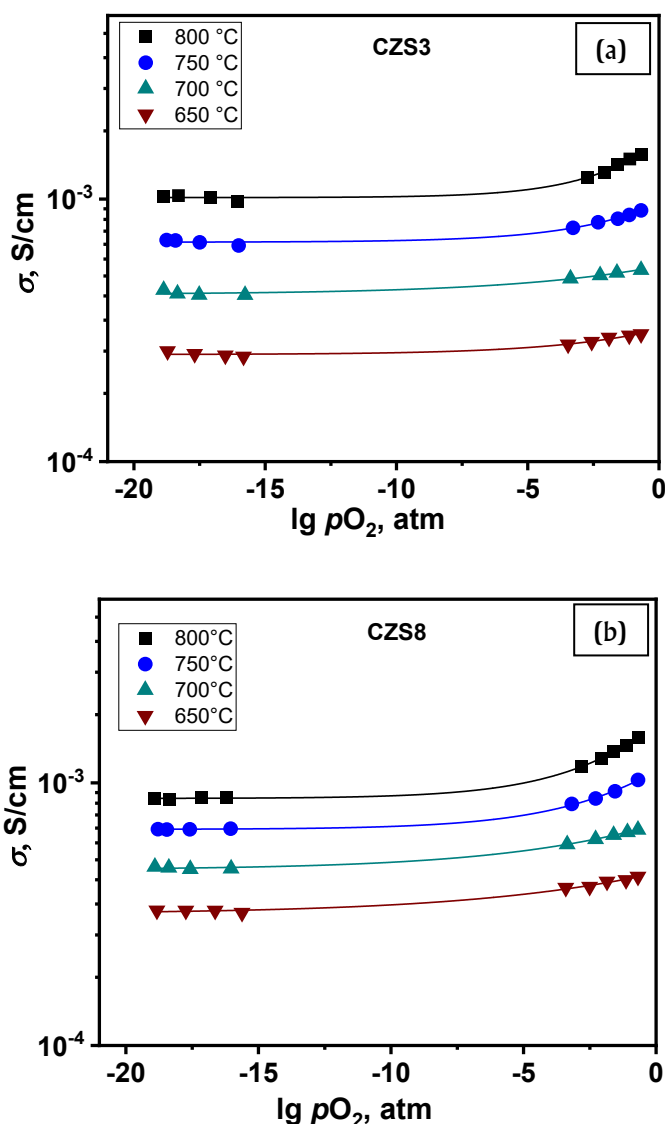
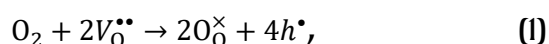


Figure 5 pO_2 -dependencies of electrical conductivity for investigated oxides: (a) CZS3, (b) CZS8.

behavior points to the presence of electron hole conductivity at high oxygen partial pressures, resulting from the interaction of oxygen with the oxide, which leads to the formation of electron holes according to



and pure ionic electrical conductivity under reductive conditions.

The obtained dependencies were fitted using the following Equation:

$$\sigma_{tot} = \sigma_{ion} + \sigma_h^0 \cdot p_{O_2}^m, \quad (2)$$

where σ_{tot} represents total conductivity, σ_{ion} is ionic conductivity, and σ_h^0 and denotes the values of hole conductivity at an oxygen partial pressure of 1 atm respectively. Consequently, ionic conductivity was determined across all temperatures. Table 2 lists the obtained values of ionic conductivity.

Subsequently, the transport numbers of ions and electron holes were calculated as follows:

$$t_{ion} = \frac{\sigma_{ion}}{\sigma_{tot}}, \quad (3)$$

$$t_{hole} = \frac{\sigma_{tot} - \sigma_{ion}}{\sigma_{tot}}. \quad (4)$$

Figure 6 shows the temperature dependencies of transport numbers for ions and electron holes in wet air conditions. One can see that ion transport numbers increase with the decrease in temperature, and it is expected that at the temperature below 600 °C CZS oxides are expected to be almost pure ionic conductors under air conditions. This is in agreement with previously reported data for CZS5 [25]. It should be noted that ion transport numbers for CZS3 are higher than those for CZS8 in the entire investigated temperature range despite the higher level of doping and, therefore, the expected higher concentration of oxygen vacancies. One of the possible reasons for such behavior, taking into account the previously estimated level of Sc solubility to be of about 0.08 mol. %, can be the formation of a low-conducting impurity phase, which concentration is too small for detection by XRD analysis, but already affects the electrical properties of the material. It can also be the reason of the increased activation energy for grain boundary conductivity for CZS8 sample, as the impurity phases are usually localized in the grain boundary region. To summarize, it can be concluded that between the investigated samples, the optimal level of doping from the point of electrical conductivity and ionic transport is 3 mol. % of Sc.

Table 2 – Ionic conductivity values for CZS oxides.

$T, ^\circ\text{C}$	$\sigma_{ion}, \text{S/cm}$	
	CZS3	CZS8
800	0.00101	0.00087
750	0.00068	0.00066
700	0.00043	0.00047
650	0.00026	0.00032

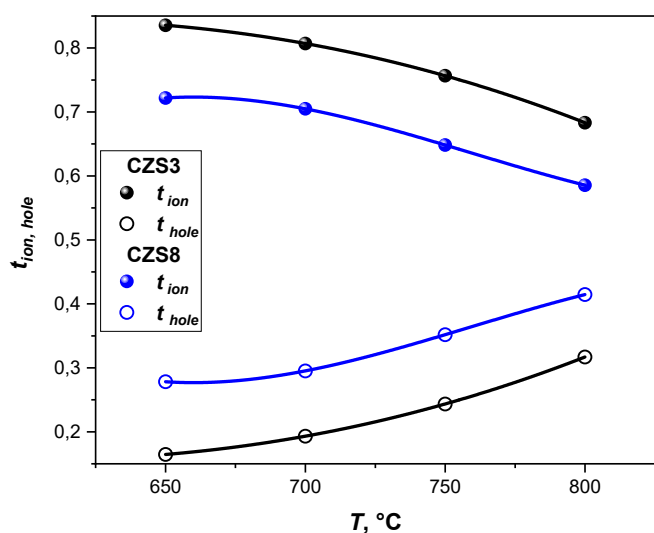


Figure 6 Transport numbers for ions and electron holes for investigated oxides in wet air.

4. Conclusions

In the course of the study, the electrical properties of Sc-doped (3 and 8 mol. % Sc) CaZrO_3 ceramics were investigated. The electrical conductivity of the oxides is comparable, reaching approximately 10^{-3} S/cm at 800 °C in a humidified air atmosphere. At temperatures below 700 °C, bulk and grain boundary contributions to total conductivity were separated. It was found that the grain boundary conductivity is lower than the bulk conductivity, thereby limiting the overall conductivity of the materials. Therefore, to enhance the electrical performance of these oxides, optimizing the ceramic microstructure to reduce the grain boundary contribution is necessary.

Using the conductivity dependencies on oxygen partial pressure, the contributions of ionic and electron hole conductivities were separated, and the corresponding transport numbers were determined. Sc-doped CaZrO_3 oxides exhibit mixed ionic-electron hole conduction in air atmosphere and are pure ionic conductors under reductive conditions. Ion transport numbers increase with the decrease in temperature, and, therefore, it is expected that at the temperature below 600 °C investigated oxides act as nearly pure ionic conductors under air conditions. Ion transport numbers for 3 mol. % Sc-doped CaZrO_3 were found to be higher than those for 8 mol. % Sc-doped CaZrO_3 . In summary, between the investigated samples, the optimal doping level from the perspective of electrical conductivity and ionic transport is 3 mol. % of Sc.

Supplementary materials

No supplementary materials are available.

Funding

This research had no external funding.

Acknowledgments

The author is grateful to Dr. V.B. Balakireva, Dr. V.P. Gorelov and Dr. A.V. Kuzmin for providing the samples for the studies. The facilities of the shared access center “Composition of Compounds” of IHTE UB RAS were used.

Author contributions

Ekaterina Antonova: Conceptualization; Investigation; Methodology; Writing – Original draft; Writing – Review & Editing; Visualization.

Conflict of interest

The authors declare no conflict of interest.

Additional information

Ekaterina Antonova, PhD, senior researcher, Laboratory of kinetics; Institute of High Temperature Electrochemistry Ural Branch of Russian Academy of Science, Ekaterinburg, Russian Federation; ORCID: [0000-0003-3902-4395](https://orcid.org/0000-0003-3902-4395); Scopus ID: [36508426000](https://scopus.org/36508426000).

References

- Irvine J, Rupp JLM, Liu G, Xu X, et al., Roadmap on inorganic perovskites for energy applications, *J. Phys.: Energy*, **3(3)** (2021) 031502. <https://doi.org/10.1088/2515-7655/abff18>
- Savchyn VP, Popov AI, Aksimentyeva OI, Klym H, et al., Cathodoluminescence characterization of polystyrene-BaZrO₃ hybrid composites, *Low Temp. Phys.*, **42(7)** (2016) 597–600. <https://doi.org/10.1063/1.4959020>
- Coondoo I, Alikin D, Abramov A, Figueiras FG, et al., Exploring the effect of low concentration of stannum in lead-free BCT-BZT piezoelectric compositions for energy related applications, *J. Alloys Compd.*, **960** (2023) 170562. <https://doi.org/10.1016/j.jallcom.2023.170562>
- Sun C, Alonso JA, Bian J, Recent advances in perovskite-type oxides for energy conversion and storage applications, *Adv. Energy Mater.*, **11(2)** (2021) 2000459. <https://doi.org/10.1002/aenm.202000459>
- Zarabi Golkhatmi S, Asghar MI, Lund PD, A review on solid oxide fuel cell durability: latest progress, mechanisms, and study tools, *Renew. Sustain. Energy Rev.*, **161** (2022) 112339. <https://doi.org/10.1016/j.rser.2022.112339>
- Iwahara H, Esaka T, Uchida H, Maeda N, Proton conduction in sintered oxides and its application to steam electrolysis for hydrogen production, *Solid State Ionics*, **3–4** (1981) 359–363. [https://doi.org/10.1016/0167-2738\(81\)90113-2](https://doi.org/10.1016/0167-2738(81)90113-2)
- Kasyanova AV, Zvonareva IA, Tarasova NA, Bi L, et al., Electrolyte materials for protonic ceramic electrochemical cells: Main limitations and potential solutions, *Materials Reports:*

- Energy, **2** (2022) 100158. <https://doi.org/10.1016/j.matre.2022.100158>
8. Duan C, Huang J, Sullivan N, O'Hayre R, Proton-conducting oxides for energy conversion and storage, *Appl. Phys. Rev.*, **7** (2020) 011314. <https://doi.org/10.1063/1.5135319>
9. Kim J, Sengodan S, Kim S, Kwon O, et al., Proton conducting oxides: A review of materials and applications for renewable energy conversion and storage, *Renew. Sustain. Energy Rev.*, **109** (2019) 606–618. <https://doi.org/10.1016/j.rser.2019.04.042>
10. Fop S, Solid oxide proton conductors beyond perovskites, *J. Mater. Chem. A*, **9** (2021) 18836. <https://doi.org/10.1039/d1ta03499e>
11. Rashid NLRM, Samat AA, Jais AA, Somalu MR, et al., Review on zirconate-cerate-based electrolytes for proton-conducting solid oxide fuel cell, *Ceram. Int.*, **46** (2019) 6605–6615. <https://doi.org/10.1016/j.ceramint.2019.01.045>
12. Danilov NA, Starostina IA, Starostin GN, Kasyanova AV, et al., Fundamental understanding and applications of protonic Y and Yb-Coped Ba(Ce,Zr)O₃ perovskites: state-of-the-art and perspectives, *Adv. Energy Mater.*, **13** (2023) 2302175. <https://doi.org/10.1002/aenm.202302175>
13. Hossain MK, Chanda R, El-Denglawey A, Emrose T, et al., Recent progress in barium zirconate proton conductors for electrochemical hydrogen device applications: A review, *Ceram. Int.*, **47** (2021) 23725–23748. <https://doi.org/10.1016/j.ceramint.2021.05.167>
14. Yajima T, Iwahara H, Koide K, Yamamoto K, CaZrO₃-type hydrogen and steam sensors: trial fabrication and their characteristics, *Sens. Actuators B: Chem.*, **5(1–4)** (1991) 145–147. [https://doi.org/10.1016/0925-4005\(91\)80235-C](https://doi.org/10.1016/0925-4005(91)80235-C)
15. Matsumoto H, Iwahara H, Hydrogen isotope cell and its application to hydrogen isotope sensing, *Solid State Ionics*, **136–137** (2000) 173–177. [https://doi.org/10.1016/S0167-2738\(00\)00308-8](https://doi.org/10.1016/S0167-2738(00)00308-8)
16. Dunyushkina LA, Smirnova EO, Smirnov SV, Kuimov VM, Plaksin SV, Microstructure, hardness, and electrical behavior of Y-doped CaZrO₃ films prepared by chemical solution deposition, *Ionics*, **19(3)** (2013) 511–515. <https://doi.org/10.1007/s11581-012-0769-x>
17. Bao J, Okuyama Y, Shi Z, Fukatsu N, Kurita N, Properties of electrical conductivity in Y-doped CaZrO₃, *Mater. Trans.*, **53(5)** (2012) 973–979. <https://doi.org/10.2320/matertrans.M2012017>
18. Bao J, Ohno H, Okuyama Y, Fukatsu N, Kurita N, Electromotive force of the high-temperature concentration cell using Al-doped CaZrO₃ as the electrolyte, *Mater. Trans.*, **53(4)** (2012) 752–759. <https://doi.org/10.2320/matertrans.M2012020>
19. Bao J, Ohno H, Kurita N, Okuyama Y, Fukatsu N, Proton conduction in Al-doped CaZrO₃, *Electrochimica Acta*, **56(3)** (2011) 1062–1068. <https://doi.org/10.1016/j.electacta.2010.10.098>
20. Zhang C, Li Y, Ding Y, Electrical properties of CaZrO₃ co-doped with Sn and Sc, *Ceram. Int.*, **51(15)** (2025) 21026–21036. <https://doi.org/10.1016/j.ceramint.2025.02.271>
21. Yajima T, Kazeoka H, Yogo T, Iwahara H, Proton conduction in sintered oxides based on CaZrO₃, *Solid State Ionics*, **47(3–4)** (1991) 271–275. [https://doi.org/10.1016/0167-2738\(91\)90249-B](https://doi.org/10.1016/0167-2738(91)90249-B)
22. Tian Z, Ruan F, Bao J, Song X, et al., Preparation and electrochemical properties of CaZr_{1-x}Sc_xO_{3-α}, *J. Electrochem. Soc.*, **166(6)** (2019) B441–B448. <https://doi.org/10.1149/2.0971904jes>
23. Huang W, Li Y, Li H, Ding Y, Ma B, Preparation and ionic conduction of CaZr_{1-x}Sc_xO_{3-α} ceramics, *Ceram. Int.*, **42(12)** (2016) 13404–13410. <https://doi.org/10.1016/j.ceramint.2016.05.117>
24. Anan'ev MV, Bershitskaya NM, Plaksin SV, Kurumchin EK, Phase equilibriums, oxygen exchange kinetics and diffusion in oxides CaZr_{1-x}Sc_xO_{3-x/2-δ}, *Russ. J. Electrochem.*, **48(9)** (2012) 879–886. <https://doi.org/10.1134/S1023193512090030>
25. Gorelov VP, Balakireva VB, Kuz'min AV, Plaksin SV, Electrical conductivity of CaZr_{1-x}Sc_xO_{3-α} (x = 0.01–0.20) in dry and humid air, *Inorg. Mater.*, **50(5)** (2014) 495–502. <https://doi.org/10.1134/S0020168514050057>
26. Balakireva VB, Gorelov VP, Dunyushkina LA, Kuz'min AV, Impact of humidity on charge transport in proton-conducting perovskites AZr_{0.95}Sc_{0.05}O_{3-α} (A = Ca, Sr, Ba) exposed to an oxidative atmosphere, *Phys. Solid State*, **61** (2019) 515–522. <https://doi.org/10.1134/S1063783419040048>
27. Gorelov VP, Balakireva VB, Kuz'min AV, Partial conductivities in perovskites CaZr_{1-x}Sc_xO_{3-α} (x = 0.03–0.20) in an oxidation atmosphere, *Phys. Solid State*, **58** (2016) 12–18. <https://doi.org/10.1134/S1063783416010145>
28. Lyagaeva J, Danilov N, Korona D, Farlenkov A, et al., Improved ceramic and electrical properties of CaZrO₃-based proton-conducting materials prepared by a new convenient combustion synthesis method, *Ceramics Int.*, **43** (2017) 7184–7192. <http://dx.doi.org/10.1016/j.ceramint.2017.03.006>